NMR Studies of Amyloid β-Peptides: Proton Assignments, Secondary Structure, and Mechanism of an α-Helix → β-Sheet Conversion for a Homologous, 28-Residue, N-Terminal Fragment

Michael G. Zagorski* and Colin J. Barrow‡

Suntory Institute for Bioorganic Research, Wakayamadai, Shimamoto-cho, Mishima-gun, Osaka 618, Japan

Received January 17, 1992; Revised Manuscript Received March 23, 1992

ABSTRACT: β-Peptide is a major component of amyloid deposits in Alzheimer's disease. We report here a proton nuclear magnetic resonance (NMR) spectroscopic investigation of a synthetic peptide that is homologous to residues 1–28 of β-peptide [abbreviated as β-(1–28)]. The β-(1–28) peptide produces insoluble β-pleated sheet structures in vitro, similar to the β-pleated sheet structures of β-peptide in amyloid deposits in vivo. For peptide solutions in the millimolar range, in aqueous solution at pH 1–4 the β-(1–28) peptide adopts a monomeric random coil structure, and at pH 4–7 the peptide rapidly precipitates from solution as an oligomeric β-sheet structure, analogous to amyloid deposition in vivo. The NMR work shown here demonstrates that the β-(1–28) peptide can adopt a monomeric α-helical conformation in aqueous trifluoroethanol solution at pH 1–4. Assignment of the complete proton NMR spectrum and the determination of the secondary structure were arrived at from interpretation of two-dimensional (2D) NMR data, primarily (1) nuclear Overhauser enhancement (NOE), (2) vicinal coupling constants between the amide (NH) and αH protons, and (3) temperature coefficients of the NH chemical shifts. The results show that at pH 1.0 and 10 °C the β-(1–28) peptide adopts an α-helical structure that spans the entire primary sequence. With increasing temperature and pH, the α-helix unfolds to produce two α-helical segments from Ala2 to Asp7 and Tyr10 to Asn27. Further increases in temperature to 35 °C cause the Ala2–Asp7 section to become random coil, while the His13–Phe20 section stays α-helical. A mechanism involving unfavorable interactions between charged groups and the α-helix macrodipole is proposed for the α-helix → β-sheet conversion observed at midrange pH.

β-Peptide is the major proteinaceous component of amyloid deposits in Alzheimer's disease (AD) and Down's syndrome (Glenner & Wong, 1984; Masters et al., 1985a). It is a small polypeptide [39–43 amino acids, see Chart I; the peptide that contains 42 residues is referred to as β-(1–42)] with ragged termini (Masters et al., 1985b). Cleavage of a larger amyloid precursor protein generates β-peptide, which later aggregates in vivo to produce insoluble β-pleated sheet structures present within extracellular amyloid deposits of AD (Kirschner et al., 1986).

Recent work has linked the accumulation of β-peptide in amyloid with the severity of dementia in AD (Flood et al., 1991). These results suggest that a buildup of β-peptide may have a direct role in the pathogenesis of AD. Therefore, a basic understanding of the molecular mechanisms of amyloidogenesis may be critical for the development of useful drugs to prevent AD.

Unfortunately, because of its extreme insolubility and high propensity to aggregate, few attempts have been made to study the solution conformations of β-peptide [for examples, see Hollosi et al. (1989) and Hilbich et al. (1991)]. We recently demonstrated (Barrow & Zagorski, 1991) that, under certain solution conditions, naturally occurring synthetic β-peptides and related fragments can exist in monomeric (nonaggregated) α-helical conformations. If solution conditions are appropriately changed, then β-peptide can rearrange from a monomeric α-helix to an oligomeric β-sheet conformation, which eventually precipitates from solution producing amyloid-like deposits.

The ability of β-peptide to exist in different conformations is dependent upon residues 1–28 [β-(1–28), Chart I], since the remaining 29–42 hydrophobic segment adopts a β-sheet conformation (Barrow & Zagorski, 1991). In addition, the synthetic β-(1–28) peptide forms amyloid-like fibrils in vitro, which morphologically resemble fibrils of natural amyloid in vivo (Kirschner et al., 1987; Gorevic et al., 1987). In view of the importance of the 1–28 segment in amyloid formation, we decided to study the β-(1–28) peptide by nuclear magnetic resonance (NMR) spectroscopy. We report here a two-dimensional (2D) NMR study of this peptide under conditions where it adopts an ordered structure (60%, v/v, trifluoroethanol-d_3). The complete proton (^{1}H) NMR spectrum has been assigned, and the secondary structure has been deduced from interpretation of nuclar Overhauser enhancement (NOE) and coupling constant data. The major result is that the peptide adopts a monomeric α-helical structure at pH 1–4 that unfolds to a partly random coil structure with increasing temperature. From analysis of the data at various temperatures, we have determined that the most stable part of the α-helix is within residues 13–20. The α-helical structure unfolds and precipitates as a β-sheet structure within the pH 4–7 range, and we propose a mechanism to explain this observation.

Materials and Methods

Sample Preparation. The β-(1–28) peptide was synthesized, purified, and characterized as described previously (Barrow & Zagorski, 1991). Samples were prepared for NMR mea-

* Address correspondence to this author at the Department of Chemistry, Case Western Reserve University, Cleveland, OH 44106–7078.
‡ Present address: Sterling Drug Inc., 9 Great Valley Parkway, Malvern, PA 19355.

0006-2960/92/0431-5621$03.00/0

Chart I

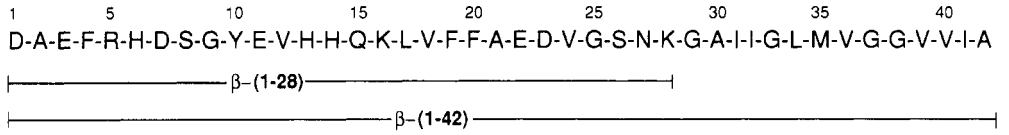

surements by dissolving the peptide (7.4 mg, 0.0021 mmol) in a solution (0.50 mL) containing a mixture by volume of either H_2O–D_2O (6:4) or H_2O–trifluoroethanol-d_3 (4:6) (trifluoroethanol-d_3 was purchased from Cambridge Isotopes, Inc., and in the text is referred to as CF_3CD_2OD or TFE-d_3). All solutions contained 10 mM sodium phosphate, 0.05 mM Na_2EDTA, and 0.05 mM NaN_3. The pH of the solutions was adjusted with a pH meter (Horiba Japan, Inc.) equipped with an electrode that fit inside the 5-mm NMR tube. The desired pH values were obtained at room temperature by adding microliter amounts of either dilute DCl or dilute NaOD. No corrections of pH readings were made for isotope effects or for the presence of TFE-d_3. As it happens, only minor differences of the pH (±0.1) were observed between aqueous buffered solutions not containing TFE and aqueous buffered solutions containing TFE. For example, when TFE (v/v, 60%) was added to an aqueous buffered solution at pH 2.29, the pH increased only slightly to 2.36. Because the difference between the two values (2.36 − 2.29 = 0.07) is within the reproducibility of our measurements, we did not attempt to correct the pH for the presence of TFE.

Procedures for NMR Data Acquisition and Analysis. All ^1H NMR spectra were obtained at 500 MHz using a General Electric GN-500 spectrometer. Two-dimensional NMR data were transferred to a Sun 3/60 data station and processed using commercially available NMR2 software (New Methods Research, Inc.). Chemical shifts are referenced to internal sodium 3-(trimethylsilyl)propionate-*2,2,3,3-d*$_4$ (TSP). Probe temperatures were calibrated using dry methanol (Van Geet, 1970).

Three types of 2D NMR experiments were utilized for assignment of the ^1H NMR spectrum of the β-(1–28) peptide: (1) double-quantum-filtered correlation spectroscopy (DQF-COSY) (Rance et al., 1983), (2) homonuclear Hartmann–Hahn spectroscopy (HOHAHA) (Bax & Davis, 1985), also known as total-correlation spectroscopy (TOCSY) (Braunschweiler & Ernst, 1983), and (3) nuclear Overhauser enhancement spectroscopy (NOESY) (Jeener et al., 1979). These experiments were run in the phase-sensitive mode with quadrature detection in both dimensions (States et al., 1982). The carrier was placed in the center of the spectrum (usually at the position of the H_2O signal), and both the H_2O signal and the residual protium absorption of TFE-d_3 were suppressed by irradiation with the proton decoupler. The irradiation was carried out during the recycle delay (2.0 s) and during the mixing time (150 ms) of the NOESY experiment. Reduction of coil lead pickup (Dykstra, 1987) was accomplished by modification of the pulse sequences to include 90°$x,y,-x,-y$ pulses for both preparation and detection (Zagorski, 1992). Before Fourier transformation, spectra were multiplied by a Lorentzian-to-Gaussian weighting factor in F_2 and a 60–90° phase-shifted sine bell in F_1. Baseline roll was reduced by careful adjustment of the intensity of the first points in F_2 and F_1 (Otting et al., 1986) and by the application of a cubic-polynomial baseline correction of the rows in the final 2D matrix. The spectral widths in both dimensions were ±2717.39 Hz, and a total of 512 increments (each consisting of 64–128 scans) were acquired with 2048 complex points for the F_1 and F_2 dimensions.

An exception to the above was a DQF-COSY experiment, which was acquired with 4096 complex points in F_2. Data from this experiment, which were used for vicinal coupling constant measurements, were zero filled once in F_2 and three times in F_1 to provide a final 4096 × 2048 matrix. Vicinal coupling constants were calculated from the separations between the positive and negative peaks in the F_2 dimension (digital resolution 1.2 Hz/point). Accurate peak positions and line widths were obtained using a bi-Gaussian surface fitting module that was present in the NMR2 software. Line-width contributions to the antiphase peak separation were removed according to Neuhaus et al. (1985), and the vicinal coupling constants between the αH and NH of each residue are summarized in Table II.

Since the TFE-d_3–H_2O (6:4) solutions contained 40% exchangeable deuterium, the intensity of the NMR signals observed for all the exchangeable protons was reduced. To make the NOE intensities (obtained by counting contours in each cross peak of NOESY spectra) comparable, we scaled the NOEs for the exchangeable amide (NH) protons; i.e., the intensities of NOEs between two neighboring NHs [an NN-(i,i+1) NOE] were increased by 40%, the intensities of NOEs between one NH and another nonexchangeable proton [i.e., an αN(i,i+1) NOE] were increased by 20%, and the intensities between two nonexchangeable protons [i.e., an αβ(i,i+3) NOE] were not altered.

For the determination of the NH temperature coefficients, the chemical shifts of the NHs were obtained from NOESY spectra acquired at 10, 15, 20, 25, 30, and 35 °C. Temperature coefficients were then taken as the slopes from a least-squares computer fitting of the chemical shifts against temperature (Table II).

Results

Preliminary Analysis. Within pH 1–4 and 7–10, solutions containing 4.1 mM β-(1–28) in TFE-d_3–H_2O were stable for several months, but if the pH was altered to within the 4–7 range, the peptide rapidly precipitated as a gel. Therefore, we could not acquire NMR data within the pH 4–7 range.

Shown in Figure 1 are one-dimensional (1D) NMR spectra acquired in TFE-d_3–H_2O (ratio, v/v, 6:4) and H_2O–D_2O (ratio, v/v 6:4). Both solvent mixtures have approximately 60% labile protium, so the intensities of the labile NH protons are comparable. Our reason for using 60% (v/v) TFE-d_3 was to maximze α-helix formation (Barrow & Zagorski, 1991).

As shown, the line widths of the NMR spectra obtained at pH 7.3 (Figure 1A,B, upper) are broadened, relative to the line widths at pH 1.0 (Figure 1C,D, lower). Previously, size exclusion chromatography data demonstrated that the β-(1–28) peptide is monomeric at pH 3.5 but both monomeric and tetrameric at pH 7.4 (Barrow et al., 1992). Together, these results suggest that a mixture of monomers and tetramers coexist at pH 7.3. In aqueous solution at pH 1.0 (Figure 1C), the line widths are narrow and the CH_3 absorptions of Ala2 and Ala21 overlap, indicating that the major conformation is monomeric and random coil. By contrast, in TFE-d_3–H_2O (6:4) at pH 1.0 (Figure 1D), the CH_3 absorptions of Ala2 and Ala21 do not overlap, indicating that the peptide adopts a folded structure.

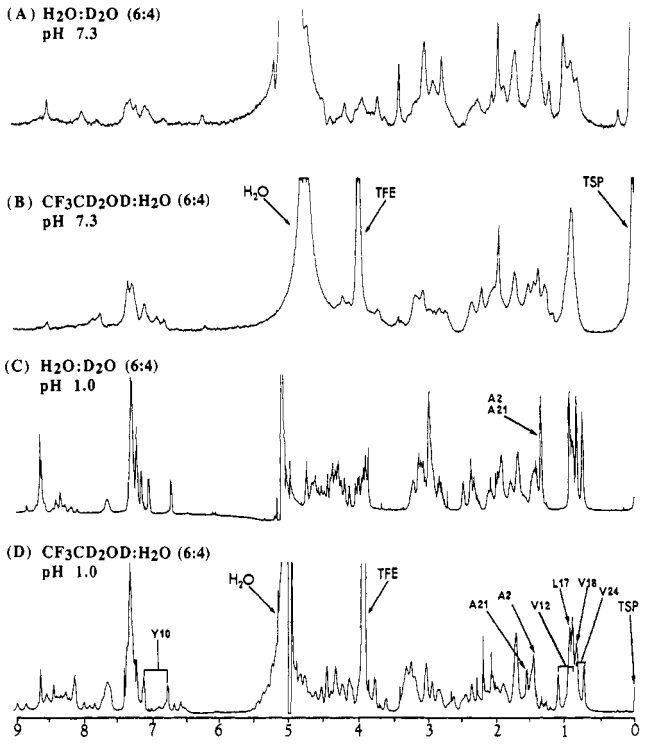

FIGURE 1: One-dimensional ^1H NMR spectra of the β-(1–28) peptide (4.1 mM) recorded at 10 °C with the solvent and pH conditions as indicated above each trace. The protium–deuterium content is 6:4 for all the spectra shown. Peak assignments for the aliphatic methyls, TSP (internal reference), and the protium absorptions of the solvents (H_2O and TFE-d_3) are shown. The solvent signals were suppressed by presaturation.

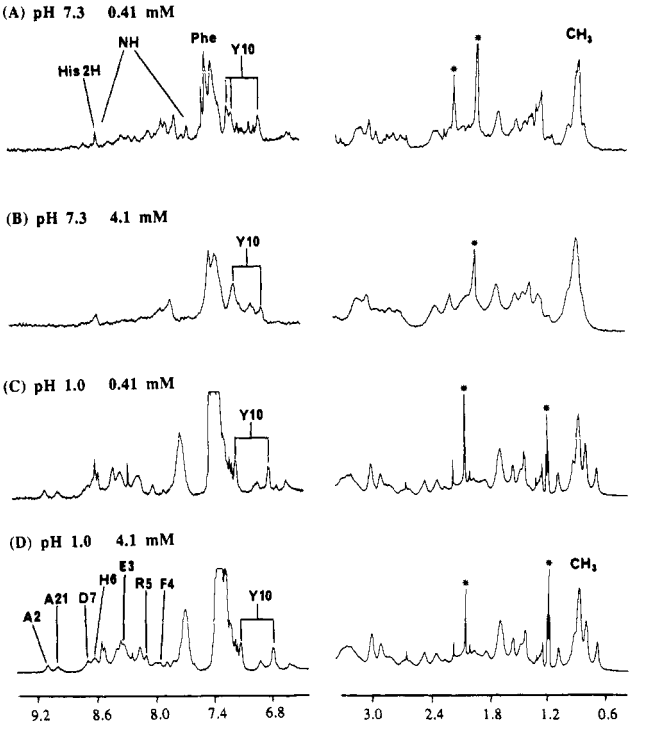

FIGURE 2: Expanded amide (left) and aliphatic (right) regions of ^1H NMR spectra acquired with different peptide concentrations. For this study, two samples were prepared: one containing 0.41 mM β-(1–28) and another containing 4.1 mM β-(1–28). Spectra in the upper two traces (A and B) were acquired at pH 7.3, while spectra in the lower two traces (C and D) were acquired at pH 1.0. All NMR data were recorded in TFE-d_3–H_2O (6:4) at 10 °C. To compensate for differences in signal/noise, approximately 20 times more scans were accumulated for the more dilute sample. At pH 1.0, spectra acquired with 0.41 and 4.1 mM peptide solutions (C and D) displayed identical line widths, and only minor differences were noted in the chemical shifts of the amides for Ala2, Ala21, Asp7, His6, Glu3, Arg5, and Phe4. At pH 7.3 many amide peaks were only observed for the more dilute sample (upper trace, A). The data were apodized with a 4.0-Hz exponential weighting factor prior to Fourier transformation. This function, together with the reduced temperature (10 °C), may also account for the somewhat broad line widths. The asterisks refer to peaks from solvent or from small amounts of EDTA present in the buffer solution.

To explore the tendency of the β-(1–28) peptide to associate, spectra were obtained with different peptide concentrations. In this experiment, 1D spectra were obtained with a sample containing 0.41 mM peptide and with another sample containing 4.1 mM peptide. Both samples were prepared in TFE-d_3–H_2O (6:4) at pH 1.0 and 7.3. At pH 7.3, many NH peaks were not visible at 4.1 mM but were visible with the solution containing 0.41 mM peptide (Figure 2A,B). In addition, the line widths of peaks in the CH_3 region were sharper in spectra obtained with 0.41 mM peptide (Figure 2A,B). By comparison, at pH 1.0 no measurable change in the line widths of the NH or CH_3 resonances was detected (Figure 2C,D). With the exception of the NHs of Ala2, Glu3, Phe4, Arg5, His6, Asp7, and Ala21, at pH 1.0 there were also no measurable changes in the chemical shifts. Also, 1D spectra obtained at pH 1.0, 2.0, 2.5, 3.0, and 3.5 showed no major differences in the line widths of the NH or CH_3 peaks. These results are consistent with a monomeric structure at pH 1–4 and mixtures of conformations at pH 7.3. Because of complications with studying peptides that contain both intra- and intermolecular interactions, we did not attempt to further study the β-(1–28) peptide at pH 7.3 and limited the remaining NMR measurements to within the pH 1–4 range.

To check for the possibility of "nascent helix" formation (Dyson et al., 1988b), we obtained NOESY data in aqueous solution without TFE. The term nascent helix has been used to describe an ensemble of interconverting extended-chain and α-helical forms present at the earliest stages of helix initiation. Most significantly, the α-helical form is detectable in 100% water solution by NMR but not by CD. For the β-(1–28) peptide in H_2O–D_2O (9:2) solution at pH 1.0 and 5 °C (optimal for possible nascent helix formation), the only interresidue connections seen in NOESY data were $\alpha N(i,i+1)$ NOEs, and no $NN(i,i+1)$ NOEs were detected. Samples containing either 4.1 or 1.0 mM peptide gave identical results. Thus, in 100% water solution no α-helical structure exists, and the peptide is largely unstructured or random coil. This agrees with the results from our CD measurements (Barrow & Zagorski, 1991).

Spin System Identification and Sequential Assignments. Shown in Chart I are the complete amino acid sequences of the β-(1–28) and β-(1–42) peptides. The sequences are unusual, and neither sequence is homologous with any proteins of known primary structure (Glenner & Wong, 1984; Flood et al., 1991). Standard procedures were used for the assignment of the proton NMR spectra of the β-(1–28) peptide (Wüthrich, 1986; Clore & Gronenborn, 1987; Bax, 1989), and below is highlighted only specific details. Table I summarizes the assignments, and in Figure 3 the observed interresidue NOE connectivities are presented.

As a first step in the analysis, the aromatic ring proton resonances were assigned. Tyr10 was easily located as a AA′XX′ spin system by intense cross peaks present in DQF-COSY and HOHAHA data, with the 3,5 ring protons being isolated and shifted upfield. The remaining aromatic ring protons of Phe4, Phe19, and Phe20, including the 4Hs of His6, His13, and His14, were nearly degenerate, even for data obtained at low temperature. This rules out any possible hy-

Table I: Proton NMR Assignments for β-(1–28) in CF_3CD_2OD–H_2O (6:4) at pH 3.0 and 25.0 °C[a]

residue	NH	αH	βH	others
D1		3.90	3.11, 3.09	
A2	8.72	4.34	1.44	
E3	8.22	4.22	2.09, 2.11	γCH_2 2.43, 2.46
F4	7.92	4.53	3.16, 3.18	2,6H 7.23; 3,5H 7.31; 4H 7.20
R5	7.93	4.14	1.83, 1.87	γCH_2 1.62, 1.63; δCH_2 3.20; εNH 7.30
H6	8.35	4.63	3.37, 3.28	2H 8.37; 4H 7.23
D7	8.48	4.76	2.97, 2.98	
S8	8.35	4.35	3.90, 3.96	
G9	8.17	3.91, 3.92		
Y10	8.03	4.31	3.15, 3.15	2,6H 7.09; 3,5H 6.78
E11	8.29	4.13	2.15, 2.29	γCH_2 2.62, 2.62
V12	8.28	3.81	2.14	γCH_3 0.94, 1.10
H13	8.07	4.33	3.28, 3.33	2H 8.52; 4 H 7.28
H14	8.49	4.28	3.09, 3.32	2H 8.57; 4H 7.37
Q15	8.31	3.96	2.18, 2.27	γCH_2 2.39; εNH_2 6.47, 6.69
K16	8.05	4.11	1.95, 1.99	γCH_2 1.51, 1.51; δCH_2 1.71, 1.73; εCH_2 2.95, 2.95; ζNH_2[b]
L17	7.67	4.26	1.73, 1.73	γCH 1.73; δCH_3 0.93, 0.93
V18	7.81	3.65	2.07	γCH_3 0.88, 0.88
F19	8.09	4.40	3.22, 3.24	2,6H 7.20; 3,5H 7.29; 4H 7.29
F20	8.38	4.31	3.21, 3.33	2,6H 7.29; 3,5H 7.31; 4H 7.29
A21	8.67	4.00	1.57	
E22	8.38	4.17	2.15, 2.22	γCH_2 2.52, 2.67
D23	8.20	4.57	2.83, 2.83	
V24	8.10	3.83	1.95	γCH_3 0.79, 0.87
G25	8.16	3.88, 3.98		
S26	7.76	4.47	3.99, 3.99	
N27	8.08	4.78	2.85, 2.86	δNH_2 6.68, 7.45
K28	7.98	4.44	1.86, 1.99	γCH_2 1.52, 1.71; δCH_2 1.49, 1.72; εCH_2 3.05, 3.05; ζNH_2 7.54

[a] Chemical shifts are reported in ppm relative to internal TSP. [b] These peaks were unassignable due to overlap or exchange with solvent.

drophobic ring stacking interactions. Weak cross peaks in HOHAHA and DQF-COSY showed long-range coupling between the 2H and 4H of the three histidine residues. The aliphatic αH and βH peaks of the aromatic residues were identified from intraresidue NOEs from the 2,6Hs of the phenylalanine and tyrosine residues and from the 4H of the histidine residues.

In the second step of the analysis, we assigned the remaining αH peaks with respect to amino acid type. Intense cross peaks in the αH region (3.6–4.8 ppm) of DQF-COSY data were diagnostic for the methyl groups of Ala2 and Ala21. In the αH region, the three valine residues were distinguished from Leu17 by the lower field position of the βHs for the valines (1.95, 2.07, and 2.14 ppm instead of 1.73 ppm). The arginine and lysine residues displayed five- and six-bond relay peaks in HOHAHA data. The terminal Lys28, which is presumably more mobile because of its location at the C-terminus, could be distinguished from Lys16 and Arg5 by intense cross peaks in DQF-COSY and weak cross peaks in NOESY spectra. The geminal βH protons of both Asp5 and Asp23 were equivalent and displayed strong cross peaks in the αH region of DQF-COSY, HOHAHA, and NOESY spectra. The αHs of the three glutamic acid residues and one glutamine residue were identified on the basis of the downfield location of the γHs relative to the βHs. The most difficult αH peaks to find were from the glycine and serine residues. $\beta N(i,i+1)$ NOEs from Ser8 and Gly25 located the NHs of Gly9 and Ser26. The αHs and βHs of Gly9 and Ser26 overlapped but could be identified by intraresidue NOEs from the NH peaks. Lastly, each αH peak was connected to an NH peak using cross peaks in DQF-COSY and HOHAHA data, thus completing the assignments of most NHs according to amino acid type.

In the final and third step of the analysis, sequence-specific resonance assignments were made on the basis of interresidue connections between backbone protons (NH, αH, βH). Figure 4 shows an expanded region of a NOESY spectrum, where cross peaks are assigned as intra- or interresidue through-space interactions. Another expanded region showing the NH–NH

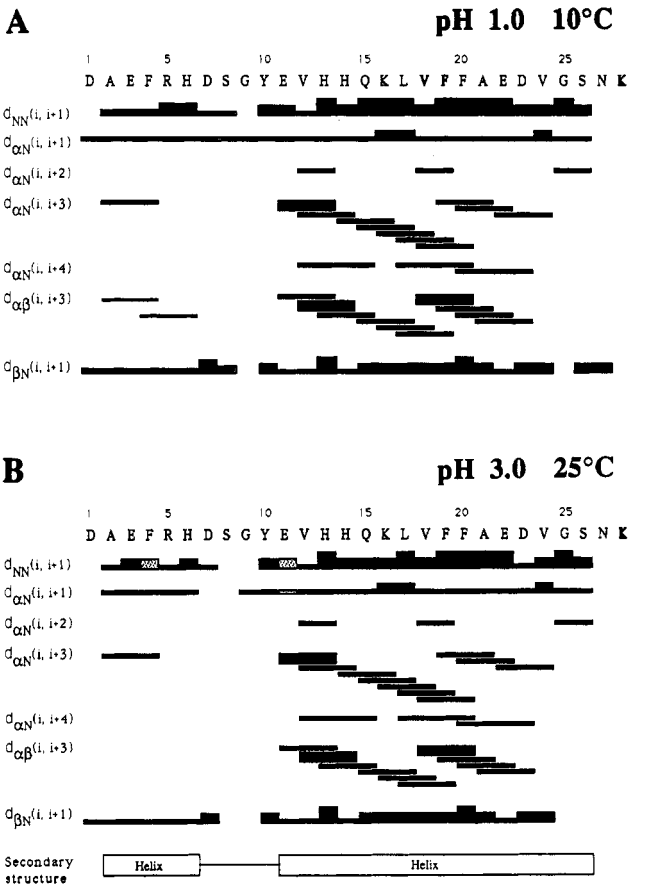

FIGURE 3: Summary of observed interresidue NOEs involving NH, αH, and βH protons. Data were taken from NOESY spectra (mixing time 150 ms) acquired in TFE-d_3–H_2O (6:4) at pH 1.0, 10.0 °C (upper, A), and at pH 3.0, 25.0 °C (lower, B). The intensities of the NOEs are reflected in the thickness of the lines. Appropriate corrections of the intensities involving the labile amide protons were made on the basis that the solvent system contains 40% exchangeable deuterium (see Materials and Methods). When peak overlap prevented assignments, NOE connections are drawn with dotted boxes.

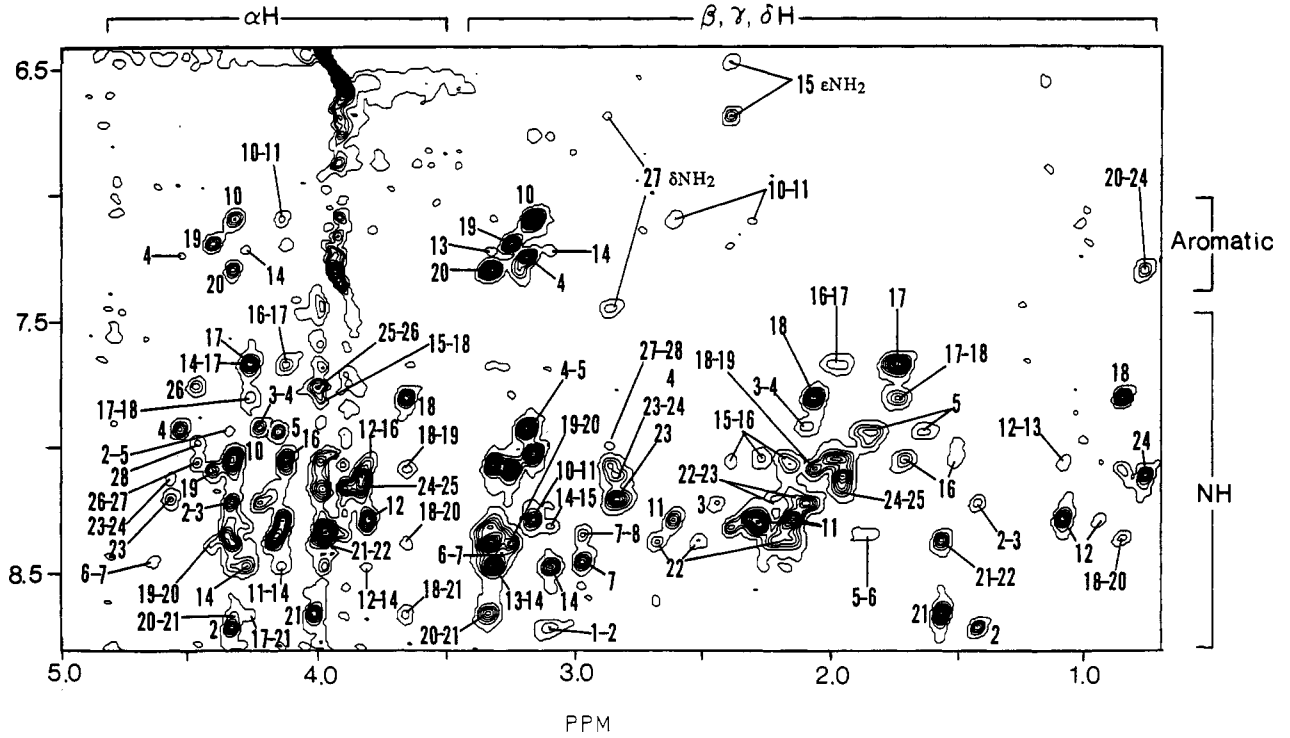

FIGURE 4: Portion of a NOESY spectra (mixing time 150 ms) for β-(1–28) at 4.1 mM concentration in TFE-d_3–H_2O (6:4), pH 3.0, and 25.0 °C, which displays NH to αH, βH, γH, and δH interactions. Also some aromatic ring proton intra- and interresidue NOEs are present in the upper section of the plot. Peaks are labeled with numbers directly next to each cross peak. Intraresidue NOEs can be distinguished from interresidue NOEs by the numbers; i.e., the peak labeled 17–21 represents an interresidue NOE between the αH of Leu17 and the NH of Ala21 [αN(i,i+3)], while the cross peak labeled 21 is representative of an intraresidue NOE between the NH and αH of Ala21. The intense band at ~3.9 ppm results from the residual protium absorption of TFE-d_3.

interresidue interactions was presented in a preliminary report (Barrow & Zagorski, 1991). We began making sequential assignments with the alanines, primarily for two reasons: (1) the chemical shifts of the alanine αH and NH peaks are accurately known, and (2) both alanine NHs appear as distinct nonoverlapped peaks and are shifted downfield relative to the remaining NH peaks (Figure 4). The NH and βHs of the alanine appearing at the lower field position displayed both NN(i,i+1) and βN(i,i+1) NOEs to a neighboring NH that was consistent with a glutamic acid residue. Thus, the NH of this alanine must be Ala2, and the NN(i,i+1) NOE and the βN(i,i+1) NOE correspond to interactions with the NH of Glu3. In contrast, Ala21 is not located adjacent to a glutamic acid residue; thus the NH appearing at the higher field position must be Ala21.

The remaining NH peaks were located by walking residue to residue along the backbone using NN(i,i+1), αH(i,i+1), and βN(i,i+1) NOEs. Once an NH was located in the NOESY spectrum, then relays (NH → αH → βH → etc.) in HOHAHA spectra were used to corroborate the assignment. If relays in HOHAHA were not present, then other NOEs were used to confirm the assignments; i.e., the 2,6H of Tyr10 had NOEs to the NH of both Tyr10 and Glu11. The only region where the assignments where difficult to obtain was within the His6-Asp7-Ser8-Gly9-Tyr10-Glu11-Val12 segment. The difficulty was due to the degeneracy of many αH and NH peaks. For example, the αHs of Ser8 and Tyr10 and the NHs of His6 and Ser8, Gly9 and Gly25, and Glu11 and Val12 all overlapped (±0.05 ppm). Additional data obtained at different pH and temperatures removed much of the overlap. The assignment of the NH of Gly9 was made on the basis of a weak-sized αN(i,i+1) NOE from its two degenerate αH protons to the NH of Tyr10. The NH of Ser8 was located by a weak-sized NN(i,i+1) NOE and a medium-sized βN-(i,i+1) NOE from the NH and βHs of Asp7.

The NH–αH coupling constants ($^3J_{HN\alpha}$) were obtained by measuring antiphase peak separations in DQF-COSY data, with removal of the line-width contributions to the observed separations (Neuhaus et al., 1985). The $^3J_{HN\alpha}$ data are summarized in Table II. The coupling constants were measured at 25 °C and not 10 °C as done for the NOE data shown in Figure 3. This procedure was followed because below 25 °C the NOE intensities increased, but the NH line widths became too broad (>7 Hz) for accurate measurements of the coupling constants.

The $^3J_{HN\alpha}$ permits a qualitative estimation of the intervening torsion angle (ϕ) between the NH and αH. Typically, α-helical segments have $^3J_{HN\alpha}$ values within 3.5–5.0 Hz, whereas β-sheet or extended-chain segments have values within 8.9–9.7 Hz (Wüthrich, 1986). Most amino acids have $^3J_{HN\alpha}$ among 5–7 Hz, consistent with ϕ of −60° to −80°. Exceptions include Val12, His14, Phe19, Phe20, and Val24 with $^3J_{HN\alpha} \leq 5.0$ Hz and Phe4, Asp7, Gly9, Glu11, Gln15, Val18, and Ser26 with $^3J_{HN\alpha} \geq 7.0$ Hz. The latter residues have $\phi > -80°$, which is not in accordance with formation of a stable α-helix and may be the result of conformational averaging between α-helical and extended-chain structures (Dyson et al., 1988b).

NOESY data obtained at pH 1.0 and 10 °C displayed additional NOEs among many side chains of the hydrophobic residues. An expanded section of a NOESY spectrum and a diagram showing the observed NOEs are presented in Figure 5. In NOESY data obtained at pH 3.0 and 25 °C, the only NOE that remained corresponded to an interaction between a CH_3 of Val24 and the 2,6Hs and Phe20. The arrows shown in Figure 5, as drawn for NOE contacts, are not stereospecific for the 2H or 6H of Phe20, since these protons are chemically shift equivalent. Besides the NOEs shown in Figure 5, other NOEs between the 2,6H of Phe20 and the βHs of Leu17, Ala21, and Val24 were also observed.

Except for Lys16, all labile side-chain NHs could be iden-

Table II: Vicinal Coupling Constants ($^3J_{HN\alpha}$) and Temperature Coefficients ($\Delta\delta/\Delta T \times 10^3$) of the Amide Protons[a]

residue	chemical shift (ppm)[b]	$^3J_{HN\alpha}$ (Hz)[c]	$-\Delta\delta/\delta T \times 10^3$ (ppm/°C)	r[d]
Ala2	8.94	6.2	8.94	0.997
Glu3	8.30	6.0	8.63	1.000
Phe4	7.97	7.5	4.76	0.994
Arg5	8.14	6.9	6.15	0.996
His6	8.52	5.3	5.94	0.997
Asp7	8.61	8.4	7.12	0.996
Ser8	8.43	5.7	4.66	0.987
Gly9	8.25	7.2	5.10	0.994
Tyr10	8.12	5.9	5.10	0.998
Glu11	8.34	7.4	5.74	0.994
Val12	8.42	3.5	11.80	1.000
His13	8.13	5.1	1.70	0.904
His14	8.55	4.4	5.53	1.000
Gln15	8.36	7.2	0.914	0.834
Lys16	8.10	5.7	1.03	0.936
Leu17	7.70	5.7	1.30	0.973
Val18	7.89	7.2	6.38	1.000
Phe19	8.19	3.3	8.54	0.994
Phe20	8.52	3.6	10.10	0.997
Ala21	8.82	5.4	12.10	1.000
Glu22	8.49	6.8	8.42	1.000
Asp23	8.27	6.3	4.17	0.987
Val24	8.25	5.0	8.92	1.000
Gly25	8.26	5.9	4.17	0.986
Ser26	7.81	7.2	1.35	0.978
Asn27	8.11	6.5	2.03	0.653
Lys28	7.98	6.5		

[a] All NMR data were acquired with a 4.1 mM sample of β-(1–28) dissolved in buffered CF_3CD_2OD–H_2O (6:4) solution at pH 1.0. Amide resonances of Asp1 and Lys28 were too weak for observation in most NOESY spectra, but the amide of Lys28 was seen in DQF-COSY spectra. Thus, only a coupling constant for Lys28 is shown. [b] Chemical shifts (estimated uncertainty ±0.01 ppm) for data obtained at 10.0 °C are shown. [c] Data used for coupling constant (estimated uncertainty ±0.6 Hz) measurements were obtained at 25.0 °C. Coupling constants for the Gly residues were measurable, since the αH proton resonances were degenerate. [d] Correlation coefficients of the fitted lines (amide chemical shift against temperature) were used for computing the temperature coefficients.

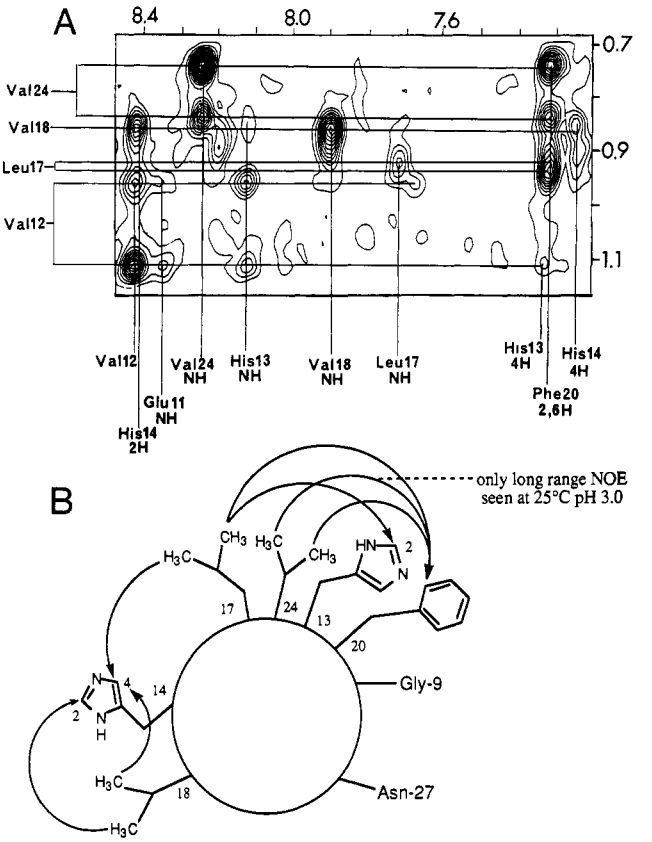

FIGURE 5: Expanded region of a NOESY spectrum (mixing time 150 ms) for β-(1–28) in TFE-d_3–H_2O (6:4), pH 1.0, and 10.0 °C (upper, A). In the right corner of the spectrum, several aromatic ring proton to aliphatic methyl group NOEs are assigned, and these interactions are illustrated with arrows in the helical wheel diagram (lower, B). Many intraresidue NOEs between the NH and methyl groups are also shown (upper, A). As noted (lower, B), at pH 3.0 and 25.0 °C none of these side-chain NOEs are present, except for a medium-sized NOE between a Val24 methyl and the 2,6 protons of Phe20 (see right section of Figure 4). The methyl groups of Leu17 and Val18 cannot be conformationally distinguished.

tified. Despite changes in temperature or pH, the ζNH_2 of Lys16 was never located, suggesting that it is always solvent exposed. The geminal side-chain amide protons of Gln15 and Asn27 interacted strongly in both NOESY and HOHAHA. Also, one NH displayed a weak-sized NOE, while the other NH displayed a medium-sized NOE, to the nearby γ- and βCH_2 groups. The ϵNH of Arg5 was easily found by linkage to the vicinal δCH_2 in DQF-COSY, HOHAHA, and NOESY. The terminal ζNH_2 of Lys28 was seen with intense cross peaks in HOHAHA, which included δ- and ϵCH_2 connections to the ζNH_2, as well as amide NH, αH, and β- and γCH_2 connections. Lys28 displayed only weak-sized intraresidue NOEs, probably due to the increased mobility from its terminal location.

With the exception of Val18 and Leu17, all CH_3 groups could be stereospecifically assigned. The two γCH_3 groups of Val18 remained equivalent, regardless of changes in pH or temperature. The major configuration in Val18 is trans, since the coupling constant between the αH and βH is 11.8 Hz (Zuiderweg et al., 1985). The two γCH_3 groups of Val12 and Val24 were stereospecifically assigned from the observation of large (11.2 and 9.6 Hz, respectively) coupling constants between the αH and the βH protons and the presence of strong NOEs from each NH to one γCH_3 and weak NOEs from each NH to the other γCH_3 (Figure 5). This establishes that the αH and βH exist in a trans configuration and that the γCH_3 showing a strong NOE to the NH is in a *pro-S* configuration, while the other γCH_3 showing a weak NOE to the NH is in the *pro-R* configuration (Zuiderweg et al., 1985). Also, intraresidue NOEs from the αH to each γCH_3 were observed, which is also consistent with a trans configuration about the αH–βH bond (Zuiderweg et al., 1985).

Temperature Dependence of NH Chemical Shifts and NH to NH NOEs. The temperature dependence of the NH chemical shifts were determined from NOESY spectra recorded at 10, 15, 20, 25, 30, and 35 °C. Except for the NH of Asn27, all the resulting chemical shifts values varied linearly with temperature; i.e., the correlation coefficients (r) obtained from the computer-fitted lines were either equal to unity or almost equal to unity. The temperature and correlation coefficients are given in Table II.

Besides His13, Gln15, Lys16, Leu17, Ser26, and Asn27, most of the temperature coefficients are very similar in magnitude. The smaller values of His13, Gln15, Lys16, Leu17, Ser26, and Asn27 indicate that the NH protons for these residues are shielded from solvent. However, the low value for Asn27 may be erroneous, since the correlation coefficient for the computed-fitted line was somewhat poor. Val12, Phe20, and Ala21 have temperature coefficients significantly large, showing very little shielding of these protons from solvent.

The intensities of the NN(i,i+1) NOEs obtained at 10 and 35 °C are compared graphically in Figure 6. This NOE, which is usually diagnostic for α-helices, is considerably re-

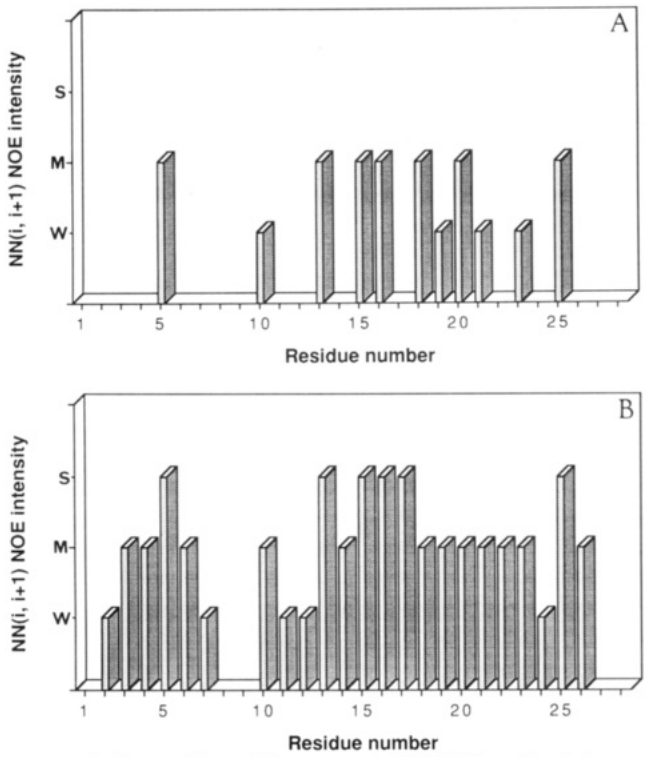

FIGURE 6: Comparison of the sequential NOE intensities between amide protons (NH) at 35 °C (upper, A) and 10 °C (lower, B). Sequential NN(i,i+1) NOEs correspond to observed through-space interactions between neighboring NHs, i.e., the NH of residue i with the NH of residue i+1. NOE intensities were categorized as strong (S), medium (M), and weak (w) by counting the contour levels in each cross peak (seen in NOESY spectra) for the observed interaction.

duced in amplitude at the higher temperature, particularly for residues at the N-terminus. At 10 °C, almost all residues have NN(i,i+1) NOEs indicative of a complete α-helical conformation. Data for terminal residues, including Ser8 and Gly9, are omitted since these NOEs were difficult to find because of peak overlap. At 35 °C, Arg5, His13, Gln15, Lys16, Leu17, Phe20, and Gly25 have NN(i,i+1) NOEs of medium-sized intensity, while Tyr10, Phe19, Ala21, and Asp23 have NOEs of weak-sized intensity.

Discussion

Nature of the Conformations Observed at pH 1–4 and 7–10. A major problem with the interpretation of the NMR data is that the β-(1–28) peptide can adopt multiple conformations in solution. Therefore, we have restricted our 2D measurements to TFE-d_3–H_2O solutions, where the peptide should adopt a predominantly α-helical conformation.

Formation of the α-helical conformation in vivo is dependent upon the ability of β-peptide to interact with a suitable membrane-like enviroment, similar to TFE. Once generated in brain tissue, we propose the β-peptide may become localized within a membrane-like environment, where it can adopt a nonaggregated α-helical conformation. In an α-helical conformation, β-peptide would remain in solution and could be transported in blood. This proposition would account for the observation of amyloid deposits containing β-peptide in tissues other than brain (Joachim et al., 1989). TFE is a membrane-mimicking solvent that encourages intramolecular hydrogen bonding, analogous to sodium dodecyl sulfate micelles or phospholipid vesicles (Nelson & Kallenbach, 1986). Recent work from our laboratories has shown that the β-(1–28) peptide has identical CD spectra in TFE–H_2O and sodium dodecyl sulfate micelles (Vassilev and Zagorski, unpublished results). In NMR studies of polypeptides, TFE–H_2O is often used to mimic membrane-like environments, and some examples include glucagon-like peptides (Gronenborn et al., 1987), alamethicin (Esposito et al., 1987), melittin (Bazzo et al., 1988), δ-hemolysin (Tappin et al., 1988), and dynorphin (Lancaster et al., 1991).

We were unable to obtain NMR data for the β-(1–28) peptide within the pH 4–7 range. In general, α-helix formation is favored at pH 1–4 and 7–10, while β-sheet formation is favored at pH 4–7 (Barrow & Zagorski, 1991). NMR solutions containing 4.1 mM β-(1–28) were stable for several months in either 100% water or TFE-d_3–H_2O (6:4) when the solution was stored at high or low pH, but when the pH was altered to 4–7, the sample precipitated as an insoluble gel. This presumably occurred because the NMR solution contained high peptide concentrations and rapidly produced the oligomeric β-sheet conformation.

One-dimensional NMR data at pH 7.3 (Figure 2A,B) show that the α-helical conformation may undergo some intermolecular association within a 0.41–4.1 mM range of peptide concentration. In contrast, CD measurements (Barrow et al., 1992) showed that within the 0.0017–0.66 mM range the α-helical content is concentration independent. Possible explanations for the broad NMR line widths observed at pH 7.3 are that some intermolecular β-sheet structures are present or that a mixture of conformations are undergoing slow interconversions within the NMR time scale. If the observed broadening is due to α-helical association, then interactions along a hydrophobic face, such as along the Leu17-Val18-Phe19-Phe20-Ala21 segment, may be responsible. Another possible explanation is that some intermolecular side-chain to backbone amide hydrogen bonding may be occurring (Bundi et al., 1978). The residues His6, His13, and His14 are good candidates as potential hydrogen bond acceptors, since they are all presumably deprotonated at pH 7.3 and can participate in hydrogen bonding to backbone amide groups (Boussard et al., 1986). If such intermolecular hydrogen bonding truly occurs, then increases in ionic strength should weaken them, thereby favoring production of monomeric α-helical structure. Indeed, Hilbich et al. (1991) observed only monomeric β-peptide structures under conditions of high salt. We are currently reexamining the effects of ionic strength upon the structural and aggregational properties of β-peptides.

Within the pH 1–4 range, 1D NMR data showed that no measurable change in the line widths was observed within a 0.41–4.1 mM range of peptide concentration, and no differences in the line widths for spectra recorded at pH 1.0, 2.0, 2.5, 3.0, 3.5, and 4.0 were noticed. In addition, apart from slight (>0.03 ppm) differences in the amide chemical shifts of Ala2, Glu3, Phe4, Arg5, His6, Asp7, and Ala21, there were no significant changes in chemical shifts. The lack of any large concentration-dependent changes in line widths or chemical shifts suggests that no further aggregation above the level of a monomer occurs at pH 1.4, which is in agreement with our CD studies (Barrow & Zagorski, 1991).

Secondary Structure Determination. Two types of structural motifs can accommodate the NMR data. One possible structure is a complete α-helix that spans the entire primary sequence (residues 2–27), and the other structure would be two α-helices (residues 2–7 and 10–27). The first structure is supported by the presence of weak-sized αN(i,i+1) and medium-sized NN(i,i+1) NOEs throughout the primary sequence (Wüthrich, 1986). Support for the second structure comes from the absence of NN(i,i+1) NOEs within the Ser8-Gly9-Tyr10 segment and the absence of medium-range

$\alpha N(i,i+3)$ and $\alpha\beta(i,i+3)$ NOEs among residues 5–10.

A third possibility is that both structures coexist in solution; that is, the complete α-helical structure (residues 2–27) is favored at low pH and low temperature, while the structure composed of two α-helices (residues 2–7 and 10–27) forms as the pH or temperature increases. In the latter structure, the Ser8-Gly9 segment is solvent exposed and serves to connect the two α-helices.

Previously, it was predicted (Kirschner et al., 1987; Gorevic et al., 1987) that a reverse turn was located within the Asp7-Ser8-Gly9-Tyr10 segment. These predictions, which were based upon the amino acid composition and did not take into account the solution conditions, are not supported by the NMR data shown here (Wüthrich, 1986; Dyson et al., 1988a). The presence of an $NN(i,i+1)$ NOE between Asp7 and Ser8 (Figure 3), the absence of any reduction in the temperature coefficient of the NH of Tyr10 (Table II), the absence of an $\alpha N(i,i+2)$ NOE from Ser8 to Tyr10, and the absence of an $NN(i,i+1)$ NOE from Gly9 to Tyr10 rule out the presence of a reverse turn within the Asp7-Ser8-Gly9-Tyr10 segment.

As expected, the amide of Asp1 could not be detected due to rapid exchange with solvent. This residue, together with the last two residues (Asn27 and Lys28), is most likely flexible in solution. The absence of any short-range interresidue NOEs between the αH and NH protons, other than $\beta N(i,i+1)$ NOEs, demonstrated the lack of any ordered structure. NOEs were observed between the βH protons of Asp1 and the NH of Ala2 (Figure 3), but at higher temperatures these NOEs became too small for detection. The same situation occurred for NOEs between the βHs of Asn27 and the NH of Lys 28.

The observed NOEs at pH 1.0 and 10 °C are similar to the observed NOEs at pH 3.0 and 25 °C (Figure 3). The major differences are that many medium-range NOEs seen at pH 1.0 and 10 °C are missing at pH 3.0 and 25 °C, in particular, within the Ala2-Glu3-Phe4-Arg5-His6-Asp7 segment. For example, the two $\alpha\beta(i,i+3)$ NOEs from Ala2 to Arg5 and from Phe4 to Asp7 are absent. However, since intraresidue αN and βN, as well as interresidue $\beta N(i,i+1)$ and $NN(i,i+1)$, NOEs were still present at pH 3.0 and 25 °C, the conformational ensemble must be heavily weighted toward an extended-chain structure (Wüthrich et al., 1984). Also, most of the larger $^3J_{HN\alpha}$ values are found in the N-terminal region (residues 2–7). The reductions in pH (3 → 1) and temperature (25 → 10 °C) thus enable the Ala2-Glu3-Phe4-Arg5-His6-Asp7 segment to shift from a predominantly extended-chain to a completely α-helical structure.

Long-range NOEs (greater than five residues apart) were not observed, indicating that the α-helical structure is nonglobular, does not fold back upon itself, and is not stabilized by hydrophobic folding. No observed temperature dependence for the chemical shifts of the aromatic ring protons indicates that hydrophobic ring stacking interactions are absent. The location of Glu11 and His14 on the same face of the α-helix may indicate that some stabilization could be obtained from an intramolecular salt bridge (Marqusee & Baldwin, 1987), but this seems unlikely because at pH 1–4 both side-chain groups of Glu11 and His14 are protonated.

With the exception of the ζNH_3^+ of Lys16, all labile side-chain NH groups could be identified. This demonstrates that in the α-helical conformation the side chain of Lys16 is solvent exposed, whereas the side chains of Arg5, Gln15, Asn27, and Lys28 are solvent shielded. It is possible that the ζNH_3^+ of Lys28 and δNH_2 of Asn27 help to stabilize the helix by participating in intrahelical hydrogen bonds (Presta & Rose, 1988). Additional stabilization of the helix at low pH would result from favorable interactions of the ζNH_3^+ of Lys28 with the helix macrodipole (Shoemaker et al., 1987).

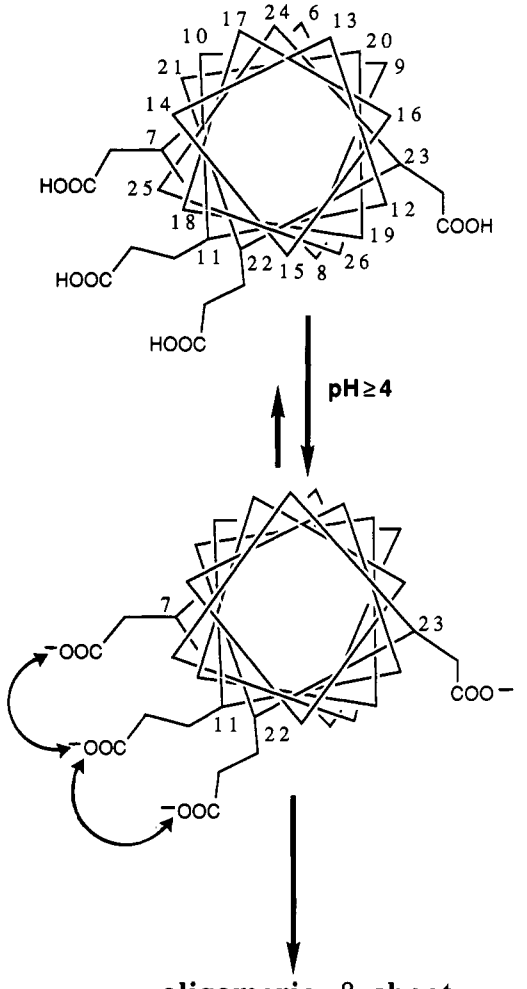

FIGURE 7: Mechanism for the α-helix (monomer) → β-sheet (oligomer) conversion of β-(1–28) as the pH is raised above 4. A helix spanning His6 to Ser26 is shown in an α-helical wheel diagram. Asp7, Glu11, Glu22, and Asp23 are expected to dissociate ($COOH \rightarrow COO^-$) above pH 4. Unfavorable interactions among the ionized carboxylates of Asp7, Glu11, and Glu22, which are located on the same face of the helix, may cause α-helix disruption.

Helix Unfolding at Elevated Temperatures. The data shown in Figures 6 and 7 establish that the α-helical content decreases with increasing temperature, which is in agreement with our CD work (Barrow et al., 1992). This shows that the α-helix is not extensively stabilized by hydrophobic interactions. The loss in α-helical structure is gradual and noncooperative, in contrast to the rapid and strong cooperative unfolding transitions seen in globular proteins (Creighton, 1984). The temperature coefficients of the amide protons of His13, Gln15, Lys16, and Leu17 are small, relative to the other amide protons, indicating that the α-helix formed by hydrogen bonding with these amides is solvent shielded. Except for Gln15, residues within the Val12–Ala21 stretch have $^3J_{HN\alpha}$ values less than 6.0 Hz, showing that ϕ is less than −60°, which is consistent with an α-helical conformation (Wüthrich, 1986).

Residues within the Val12–Ala21 sequence also retain $NN(i,i+1)$ NOEs at elevated temperature. Since the $NN(i,i+1)$ NOE is diagnostic for helices, this implies that the helix is thermodynamically most stable within the Val12–Ala21 region. A problem with this interpretation is that many NOEs could be weaker at the higher temperatures because of the

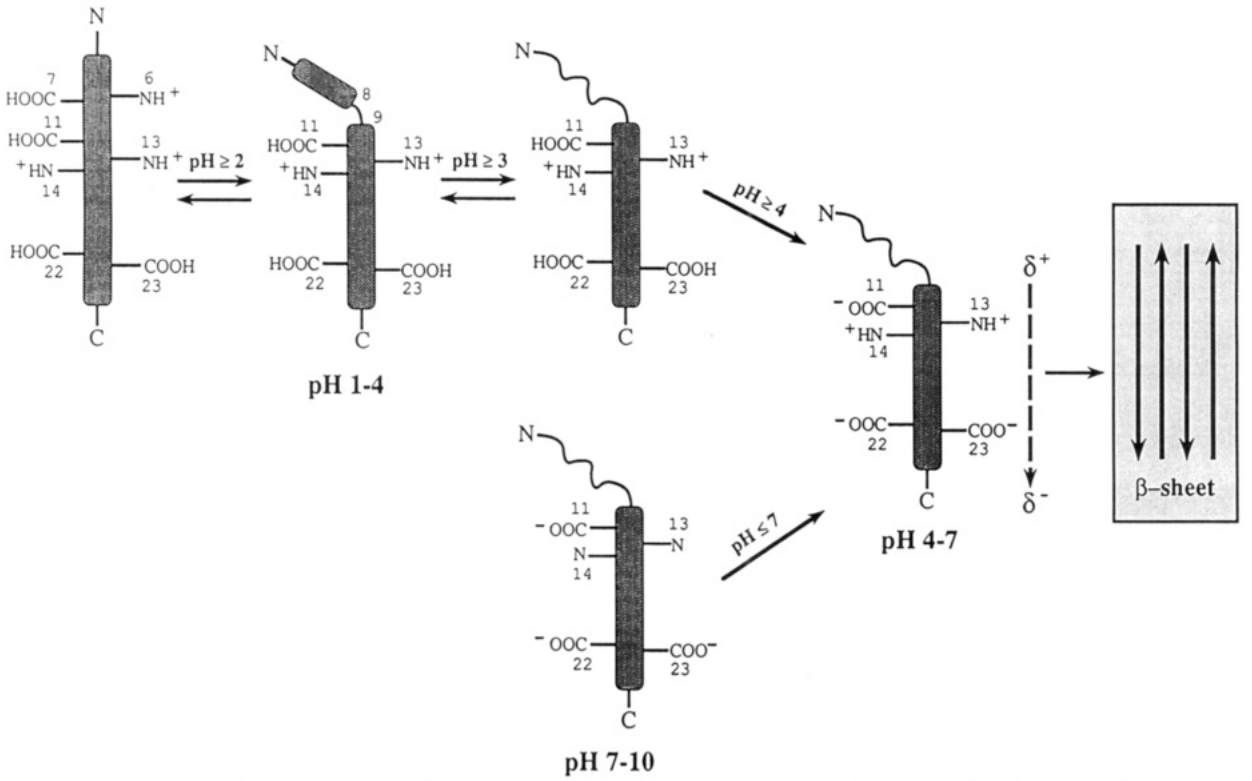

FIGURE 8: Mechanism for the α-helix (monomer) → β-sheet (oligomer) conversion of β-(1–28) as the pH is raised above 4 or lowered below 7. The α-helical regions are drawn with darkened cylinders, and the antiparallel β-sheet arrangement of β-peptide in amyloid deposits is drawn with arrows running in opposite directions. The side chains of Asp7, Glu11, Glu22, and Asp23 are expected to deprotonate (COOH → COO^-) above pH 4, and the side chains of His6, His13, and His14 are expected to become protonated (3N → $3NH^+$) below pH 7. We hypothesize that unfavorable electrostatic interactions between charged groups and the α-helix macrodipole destabilize the α-helix to promote its disruption (Shoemaker et al., 1987). If the peptide concentration is relatively dilute, then the process is reversible, for example, by lowering the pH below 4. But if the peptide concentration reaches a certain critically high value, then α-helix breakdown will be accompanied by a rearrangement to an oligomeric β-sheet. This latter process may be analogous to formation of the β-pleated sheet structures of β-peptide in amyloid deposits.

reduced viscosity and reduced correlation times. This makes direct comparison of NOE data obtained at 10 and 35 °C difficult. Nonetheless, direct comparison of NOE intensities within the 35 °C data alone is possible (Figure 6A, upper), and this analysis shows that retention of the α-helical structure occurs among residues 13–25.

Within the N-terminal region, only one NN(i,i+1) NOE between Arg5 and His6 remains at 35 °C (Figure 6A, upper), indicating that the helix unfolds faster in this region of the peptide. In the β-sheet conformation, Hilbich et al. (1991) noted that the N-terminal residues 1–9 are weakly hydrogen bonded and are not necessary for amyloid fibril formation. Moreover, in amyloid deposits many N-terminal residues are usually missing (Masters et al., 1985a), with the major component (64% total) lacking Asp1–Ala2–Glu3 (Masters et al., 1985b). More recent work has shown that a synthetic β-(6–25) peptide can assemble into β-pleated sheet fibrils characteristic of natural amyloid (Fraser et al., 1991a). Therefore, the N-terminal residues appear to be unimportant for the formation of regular structure within β-peptide.

The oligomeric β-pleated sheet structure within amyloid deposits is highly stabilized, perhaps by hydrophobic interactions between residues distant in the sequence. In contrast, the α-helical structure is under rapid exchange with unfolded states and is not stabilized by hydrophobic interactions. An exception, however, for the α-helical structure is the Val24–Phe20 NOE interaction (Figure 5), as this interaction persists at higher temperatures. Similar hydrophobic clustering (i,i+4) was presumed to be important in the stabilization of α-helices in globular proteins, as well as having a separate role in the formation of α-helices during protein folding (Lim, 1974a,b).

Hydrophobic residues within the His13-His14-Gln15-Lys16-Leu17-Val18-Phe19-Phe20 segment unfold last when the pH or temperature is increased. Residues within this section are likewise critical to the formation of stable amyloid-like deposits. For example, Kirschner et al. (1987) suggested that the sequence 11–24 of β-peptide contains the critical information which species an antiparallel β-sheet conformation as found in amyloid deposits, and the Lys16-Leu17-Val18-Phe19-Phe20-Ala21-Glu22 sequence is unique for β-peptide (Flood et al., 1991). β-Peptides with Phe19, Phe20, or Lys16 (Kirschner et al., 1987) substituted do not form amyloid filaments in vitro (Hilbich et al., 1991), demonstrating that this region is important for stabilization of the β-pleated sheet in amyloid deposits. This region is also important for binding to membrane-like receptors and induction of amnestic effects (Flood et al., 1991). This region is particularly stable in the α-helical structure, as many interresidue NOEs are observed between Leu17 and Val24–Phe20 (Figure 5), and the lowest $^3J_{HN\alpha}$ values are observed for Phe19 and Phe20.

Helix Unfolding at Midrange pH 4–7. The change in structure (α-helix → random coil → β-sheet) at midrange pH values begins with α-helix unfolding and must be related to the presence of ionizable groups. Between pH 4 and pH 7, the side chains of aspartic acid and glutamic acid residues ionize at pH 3 → 5, while the side chains of histidine residues ionize at pH 8 → 5 (Shoemaker et al., 1987), showing that one or more of these residues are involved in disruption of the α-helix. The pH profile indicates that dissociation of a single residue is not responsible for α-helix breakdown (data not shown); therefore, ionization of at least two side chains of

Asp1, Glu3, His6, Asp7, Glu11, His13, His14, Glu22, and Asp23 results in the disruption of the α-helix.

Ionization of aspartic acid, glutamic acid, and histidine residues makes many interactions possible. Ion pair interactions, such as Glu···His ion pair formation, would be expected to stabilize α-helix formation at pH 4–7 (Marqusee & Baldwin, 1987). However, for the β-(1–28) peptide we observe a decrease in α-helix stability within this pH region, implying that ion pair interactions do not make an important contribution to α-helix stability. Unfavorable electrostatic repulsions among the ionized carboxylates may contribute to α-helix disruption. As shown in Figure 7, examination of the α-helical wheel projection (Schiffer & Edmundson, 1967) for an α-helix shows that Asp7, Glu11, and Glu22 reside on the same face, which was also confirmed by model building a complete α-helix for the β-(1–28) peptide. Once the side-chain carboxylic acid groups of these residues ionize above pH 4, the unfavorable electrostatic repulsions among the ionized carboxylates may promote α-helix disruption. A similar explanation was used to explain the related α-helix → random coil conversion for poly(L-glutamic acid) (Doty et al., 1957). However, unlike poly(L-glutamic acid), the distances between the side-chain carboxylates in β-(1–28), as well as the repulsive energies involved, are probably not by themselves large enough to cause α-helix unfolding. Also, this mechanism does not explain why the α-helix is stabilized above pH 7.

The largest contributors to α-helix destabilization at pH 4–7 are probably unfavorable interactions between charged groups and the α-helix macrodipole. Recently, to account for the stability of α-helices in isolated peptides, a mechanism that involves a charge-group effect was proposed (Shoemaker et al., 1987), where electrostatic interactions between one pole of the α-helix macrodipole and a nearby charged group favor α-helix formation if the two charges are of opposite sign and oppose α-helix formation if they are of like sign. For the β-(1–28) peptide, the presence of the negatively charged Glu22 and Asp23 near the C-terminus will, therefore, oppose α-helix formation above pH 4. This mechanism (Figure 8) would also account for α-helix disruption as the pH is lowered below 7, since His6 will become protonated and interact unfavorably with the N-terminus. Recent work from our laboratories (Vassilev and Zagorski, unpublished observations) using β-(1–28) peptides with Glu11 and Glu22 substituted for uncharged residues also lends support to the mechanism outlined in Figure 8.

Knowledge of the extrinsic solution conditions which govern the proclivity of β-peptide to adopt a β-sheet structure, as found in amyloid deposits (Kirschner et al., 1986), rather than the more soluble α-helical structure, is extremely important. In this regard, our discovery that the secondary structures of the amyloid β-peptides are strongly dependent upon pH (Barrow & Zagorski, 1991) may provide a therapeutic means to slow down amyloid formation in AD. Regardless of whether β-peptide is in aqueous solution alone or in aqueous solution containing the membrane-mimicking TFE, it will eventually adopt an oligomeric β-sheet structure in solution at pH 4–7, at a rate which is dependent upon the peptide concentration (Barrow & Zagorski, 1991; Barrow et al., 1992). The β-sheet structure in solution is most likely a precursor to the insoluble β-pleated sheet structure found in amyloid deposits of AD. Recently, Yates et al. (1990) have demonstrated that brains from patients who die after AD are more acidic (pH 6.6) than brains from patients who die without AD (pH 7.1). Most significantly, recent work from our laboratories (Barrow et al., 1992) has shown that the rate of β-sheet production and precipitation for β-peptide is greater at pH 6.6 than at pH 7.1, and we propose that a similar drop in pH (7.1 → 6.6) may accelerate amyloid production in AD. Moreover, once precipitation has begun, restoring the pH (6.6 → 7.1) may not prevent further β-sheet production and precipitation. Many events in vivo, such as a loss of oxygen to cerebral tissues, can cause localized drops in pH (Gilboe et al., 1986). Related work from two other leading laboratories (Fraser et al., 1991b; Burdick et al., 1992) also supports our proposition that indeed an acidic pH environment may be important to the pathogenesis of amyloid formation in AD.

Additional studies with other peptides that contain amino acid substitutions or N- and C-terminal derivatization need to be undertaken before the factors which govern the α-helix → random coil → β-sheet conversion can be addressed more specifically.

Conclusions

This study has provided information on a molecular level about the α-helical conformation of the β-(1–28) peptide and the stability of different amino acid regions to pH, concentration, and temperature. The ability of the β-(1–28) peptide to exist in a nonaggregated α-helical conformation could have implications to the in vivo transport and deposition of β-amyloid. Knowledge of the three-dimensional solution structure of β-peptide may provide a useful target for the design of drugs to prevent amyloid deposition in AD. We believe that the NMR assignments in this paper provide a foundation for further studies of the structure, dynamics, and mechanism of amyloidogenesis of β-peptide.

Acknowledgments

We thank Drs. Vassil Vassilev (SUNBOR), Takashi Iwashita (SUNBOR), and Koji Nakanishi (Director, SUNBOR) for many helpful discussions. We also are extremely grateful to Mr. Hajime Chiba (JEOL Trading, Inc.) for assistance with using the NMR2 software.

Registry No. β-(1–28), 109770-29-8.

References

Barrow, C. J., & Zagorski, M. G. (1991) *Science 253*, 179–182.

Barrow, C. J., Yasuda, A., Kenny, P. T. M., & Zagorski, M. G. (1992) *J. Mol. Biol.* (in press).

Bax, A. (1989) *Annu. Rev. Biochem. 58*, 223–256.

Bax, A., & Davis, D. G. (1985) *J. Am. Chem. Soc. 107*, 2820–2821.

Bazzo, R., Tappin, M. J., Pastore, A., Harvey, T. S., Carver, J. A., & Campbell, I. D. (1988) *Eur. J. Biochem. 173*, 139–146.

Boussard, G., Marraud, M., & Aubry, A. (1986) *Int. J. Pept. Protein Res. 28*, 508–517.

Braunschweiler, L., & Ernst, R. R. (1983) *J. Magn. Reson. 53*, 521–528.

Bundi, A., Andreatta, R. H., & Wüthrich, K. (1978) *Eur. J. Biochem. 91*, 201–208.

Burdick, D., Soreghan, B., Kwon, M., Kosmoski, J., Knauer, M., Henschen, A., Yates, J., Cotman, C., & Glabe, C. (1992) *J. Biol. Chem. 267*, 546–554.

Castano, E. M., & Frangione, B. (1988) *Lab. Invest. 58*, 122–132.

Clore, G. M., & Gronenborn, A. M. (1987) *Protein Eng. 1*, 275–288.

Creighton, T. E. (1984) *Proteins*, Freeman, New York.

Doty, P., Wada, A., Yang, J. T., & Blout, E. R. (1957) *J. Polym. Sci. 23*, 851–861.
Dykstra, R. (1987) *J. Magn. Reson. 72*, 162–167.
Dyson, H. J., Rance, M., Houghten, R. A., Lerner, R. A., & Wright, P. E. (1988a) *J. Mol. Biol. 201*, 161–200.
Dyson, H. J., Rance, M., Houghten, R. A., Wright, P. E., & Lerner, R. A. (1988b) *J. Mol. Biol. 201*, 201–217.
Esposito, G., Carver, J. A., Boyd, J., & Campbell, I. D. (1987) *Biochemistry 26*, 1043–1050.
Flood, J. F., Morley, J. E., & Roberts, E. (1991) *Proc. Natl. Acad. Sci. U.S.A. 88*, 3363–3366.
Fraser, P. E., Duffy, L. K., O'Malley, M. B., Nguyen, J. T., Inouye, H., & Kirschner, D. A. (1991a) *J. Neursci. Res. 28*, 474–485.
Fraser, P. E., Nguyen, J. T., Surewicz, W. K., & Kirschner, D. A. (1991b) *Biophys. J. 60*, 1190–1201.
Gilboe, D. D., Kinter, D. B., Emoto, S. E., & Fitzpatrick, J. H., Jr. (1986) in *Pharmacology of Cerebral Ischemia* (Krieglstein, J., Ed.) pp 119–130, Elsevier Science Publishers, New York.
Glenner, G. G., & Wong, C. W. (1984) *Biochem. Biophys. Res. Commun. 120*, 885–890.
Gorevic, P. D., Castano, E. M., Sarma, R., & Frangione, B. (1987) *Biochem. Biophys. Res. Commun. 147*, 854–862.
Gronenborn, A. M., Bovermann, G., & Clore, G. M. (1987) *FEBS Lett. 215*, 88–93.
Hilbich, C., Kisters-Woike, B., Reed, J., Masters, C. L., & Beyreuther, K. (1991) *J. Mol. Biol. 218*, 149–163.
Hirsh, J. (1991) *N. Engl. J. Med. 324*, 1565–1574.
Hollosi, M., Otvos, L., Kajtar, J., Percell, A., & Lee, V. M.-Y. (1989) *Pept. Res. 2*, 109–113.
Jeener, J., Meier, B. H., Bachmann, P., & Ernst, R. R. (1979) *J. Chem. Phys. 71*, 4546–4553.
Joachim, C. L., Mori, H., & Selkoe, D. J. (1989) *Nature 341*, 226–230.
Kirschner, D. A., Abraham, C., & Selkoe, D. J. (1986) *Proc. Natl. Acad. Sci. U.S.A. 83*, 503–507.
Kirschner, D. A., Inouye, H., Duffy, L. K., Sinclair, A., Lind, M., & Selkoe, D. J. (1987) *Proc. Natl. Acad. Sci. U.S.A. 84*, 6953–6957.
Lancaster, C. R. D., Mishra, P. K., Hughes, D. W., St.-Pierre, S. A., Bothner-By, A. A., & Epand, R. M. (1991) *Biochemistry 30*, 4715–4726.
Lim, V. I. (1974a) *J. Mol. Biol. 88*, 857–872.
Lim, V. I. (1974b) *J. Mol. Biol. 88*, 873–894.
Marqusee, S., & Baldwin, R. L. (1987) *Proc. Natl. Acad. Sci. U.S.A. 84*, 8898–8902.
Masters, C. L., Simms, G., Weinman, N. A., Multhaup, G., McDonald, B. L., & Beyreuther, K. (1985a) *Proc. Natl. Acad. Sci. U.S.A. 82*, 4245–4249.
Masters, C. L., Multhaup, G., Simms, G., Pottgiesser, J., Martins, R. N., & Beyreuther, K. (1985b) *EMBO J. 4*, 2757–2763.
Nelson, J. W., & Kallenbach, N. R. (1986) *Proteins: Struct., Funct., Genet. 1*, 211–217.
Neuhaus, D., Wagner, G., Vasak, M., Kägi, J. H. R., & Wüthrich, K. (1985) *Eur. J. Biochem. 151*, 257–273.
Otting, G., Widmer, H., Wagner, G., & Wüthrich, K. (1986) *J. Magn. Reson. 66*, 187–193.
Presta, L. G., & Rose, G. D. (1988) *Science 240*, 1632–1641.
Rance, M., Sørensen, O. W., Bodenhausen, G., Wagner, G., Ernst, R. R., & Wüthrich, K. (1983) *Biochem. Biophys. Res. Commun. 117*, 479–485.
Schiffer, M., & Edmundson, A. B. (1967) *Biophys. J. 7*, 121–135.
Schulz, G. E., & Schirmer, R. H. (1979) *Principles of Protein Structure*, p 30, Springer-Verlag, New York.
Shoemaker, K. R., Kim, P. S., York, E. J., Stewart, J. M., & Baldwin, R. L. (1987) *Nature 326*, 563–567.
Snow, A. D., Mar, H., Nochlin, D., Kimata, K., Kato, M., Suzuki, S., Hassell, J., & Wright, T. N. (1988) *Am. J. Pathol. 133*, 456–463.
States, D. J., Haberkorn, R. A., & Ruben, D. J. (1982) *J. Magn. Reson. 48*, 286–292.
Tappin, M. J., Pastore, A., Norton, R. S., Freer, J. H., & Campbell, I. D. (1988) *Biochemistry 27*, 1643–1647.
Van Geet, A. L. (1970) *Anal. Chem. 42*, 679–680.
Whinna, H. C., Blinder, M. A., Szewczyk, M., Tollefsen, D. M., & Church, F. C. (1991) *J. Biol. Chem. 266*, 8129–8135.
Wüthrich, K. (1986) *NMR of Proteins and Nucleic Acids*, Wiley, New York.
Wüthrich, K., Spitzfaden, C., Memmert, K., Widmer, H., & Wider, G. (1991) *FEBS Lett. 285*, 237–247.
Wüthrich, K., Billeter, M., & Braun, W. (1984) *J. Mol. Biol. 180*, 715–740.
Yates, C. M., Butterworth, J., Tennant, M. C., & Gordon, A. (1990) *J. Neurochem. 55*, 1624–1630.
Zagorski, M. G. (1992) *J. Magn. Reson.* (in press).
Zuiderweg, E. R. P., Boelens, R., & Kaptein, R. (1985) *Biopolymers 24*, 601–611.